Experimental and Numerical Research for Fluidization Behaviors in a Gas–Solid Acoustic Fluidized Bed

Changqing Cao, Shuqin Dong, Yanan Zhao, and Qingjie Guo
Key Laboratory of Clean Chemical Process, College of Chemical Engineering,
Qingdao University of Science and Technology, Qingdao 266042, P.R. China

DOI 10.1002/aic.12115
Published online November 17, 2009 in Wiley InterScience (www.interscience.wiley.com).

The effects of sound assistance on fluidization behaviors were systematically investigated in a gas–solid acoustic fluidized bed. A model modified from Syamlal–O'Brien drag model was established. The original solid momentum equation was developed and an acoustic model was also proposed. The radial particle volume fraction, axial root-mean-square of bed pressure drop, granular temperature, and particle velocity in gas–solid acoustic fluidized bed were simulated using computational fluid dynamics (CFD) code Fluent 6.2. The results showed that radial particle volume fraction increased using modified drag model compared with that using the original one. Radial particle volume fraction was revealed as a parabolic concentration profile. Axial particle volume fraction decreased with the increasing bed height. The granular temperature increased with increasing sound pressure level. It showed that simulation values using CFD code Fluent 6.2 were in agreement with the experimental data. © 2009 American Institute of Chemical Engineers *AIChE J,* 56: 1726–1736, 2010
Keywords: gas–solid fluidized bed, acoustic, sound pressure level, drag model

Introduction

Fluidized bed reactors are widely used in various industrial operations, including chemical, petroleum, mineral, and pharmaceutical industries. Powder is fluidized when an upward gas flow balances its weight, producing bed expansion as the gas stream enlarges the particle interstices. The fluidization degree decreases with decreasing the particle size due to strong interparticle forces including van der Waals adhesion forces, electrostatic attractive forces, liquid bridges, hydrogen bonds, and form-closed bonds. Homogeneous fluidization is characteristic for most beds containing Geldart type A particles. However, this homogeneous state can be disrupted by instabilities and large numbers of bubbles, which will increase heterogeneous structure and decrease gas–solid contacting probability.[1] It is significant to develop processing technologies, which can handle effectively large qualities of microparticles. Morse[2] proved that the acoustic field can enhance fluidization of fine powders. Levy et al.[3] found that bed expansion and bubble frequency were influenced intensively by sound pressure levels using 4.0×10^{-5} m coal fly ash as bed material in an acoustic fluidized bed. Guo et al.[4] investigated the effect of sound frequency on minimum fluidization velocity with micron and nanoparticles. They pointed out that minimum fluidization velocity initially decreased and then increased with increasing sound frequency. At the same sound frequency, the fluidization quality of nanoparticles can be improved significantly with increasing sound pressure level (100–103.4 dB). However, the experiments in sound-assisted fluidized bed with Geldart type A particles were much less than that with Geldart type C particles.[5,6] There were few studies simulating the fluid dynamics of acoustic fluidized bed operated with Geldart A particles.[5,6]

Computational fluid dynamics (CFD) offers a new approach to understand the complex phenomena that occur

Correspondence concerning this article should be addressed to C. Cao at ccqcdm@163.com.

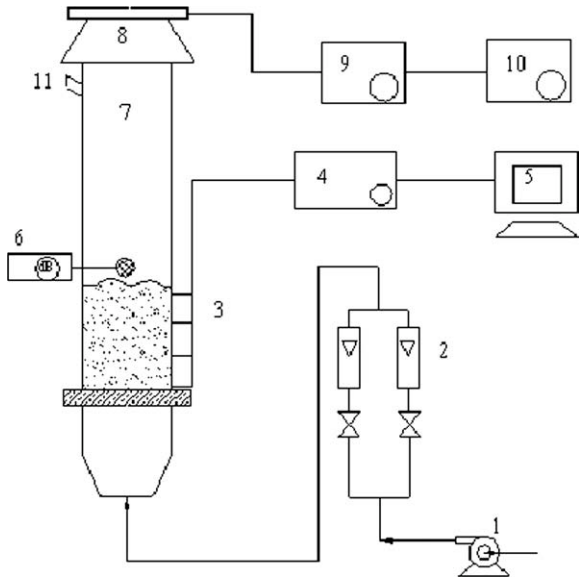

Figure 1. Experimental apparatus.

1, air compressor; 2, rotor flow meter; 3, fiber optic probe; 4, particles velocity measurer; 5, computer; 6, sound meter; 7, fluidized bed; 8, loudspeaker; 9, sound amplifier; 10, signal generator; 11, vent.

between gas phase and particles.[7–9] The drag force between gas phase and particles is one of the dominant forces in a fluidized bed. The drag laws are often developed empirically. Such general drag correlations cannot predict the drag force precisely. The main reason is that the accurate information, such as particle size and shape distributions, operation gas velocity, and so on, is not contained in the models. Zimmermann modified Syamlal–O'Brien drag model to predict the expected bubbling fluidization behavior based on the minimum fluidization conditions of the FCC particles.[8] Their results showed that the bed expansion was in disagreement with the experimental data.

In this work, Syamlal–O'Brien drag model was modified based on the operation gas velocity and the physical properties of FCC particles. An acoustic model is compiled into the CFD software based on the extra particle vibration velocity and particle momentum generated by sound assistance. The purpose of this study is to establish an acoustic model and validate the model using experimental measurements.

Experimental Arrangement

Experiments were carried out in a Perspex column with the sound-assisted fluidization system, as shown in Figure 1. The bed is 0.14 m in diameter and 1.60 m in height. The distributor is a porous glass plate with a thickness of 0.002 m and a pore size of 0.001 m. An ultrafine mesh filter was located at both the distributor and the gas outlet. A WY32003 signal generator was used to produce electric pulses with various waveforms, such as sine waves and triangle waves, whose frequency ranged from 0.001 to 3×10^6 Hz. The electric signal was then amplified with a sound amplifier and sent to a loudspeaker installed on top of the fluidized bed. A precision sound pressure level meter (CENTER, type 320) was used to measure the sound pressure level in the fluidized bed, with a 130 dB maximum sound pressure level to be measured and 1.5 dB precision. The sound meter was calibrated before starting tests, and it was found to be accurate within 0.5%. A fiber optic probe system (PV-6A, CAS) was used to measure the solid volume fractions and the principle of the fiber optic probe system was shown in the literature.[10]

Experiments were conducted at room conditions. Air was supplied with a compressor as the fluidization gas. The gas flow rate was measured and adjusted by two rotor flowmeters. The superficial gas velocity (U_G) is varied from 0.01 to 0.1 m/s. The solid particles used in this study are FCC particles with an average diameter of 8.153×10^{-5} m. The gas and solid physical properties used are given in Table 1.

The bed was prefilled with particles. The experiments were performed by fluidizing the particles with high air flow rate first. The bed was resembled a vigorously boiling, turbulent-like fluid. Then, the air flow rate was decreased gradually to avoid the particles being elutriated from the bed. The air velocity was set as 0.045 m/s to investigate the fluidization behaviors of acoustic fluidized bed. This work is devoted to investigate the dynamical behavior of sound-assisted fluidized bed from parameters such as gas–solid distribution, bubble characteristics, granular temperature, RMS of bed pressure drop, and particle velocity.

Numerical Models

Eulerian-granular model was used to simulate fluidization behaviors in the acoustic gas–solid fluidized bed. The approach regards the dispersed phases as interpenetrating continua where the local instantaneous equations are averaged in a suitable way to allow coarser grids and longer time steps being used in numerical simulations. Because of its obvious computational advantage, the Eulerian two-fluid modeling approach was applied instead of Euler–Lagrangian approach on the assumption that the gas–solid flow system has laminar, unsteady flow patterns.[11]

Governing equations

The governing equations for gas–solid system consist of a set of continuity and momentum equations for each phase under the Eulerian multiphase model.

The continuity equation for continuous as well as dispersed phases is:

Table 1. Gas and Solid Physical Properties

Parameters	Value/Comment
Gas	
Type	Air
Temperature	Ambient
Density (kg/m^3)	1.225
Viscosity (kg/ms)	1.8×10^{-5}
Particle	
Type	FCC
Size (m)	8.153×10^{-5}
Density (kg/m^3)	1807.5

$$\frac{\partial}{\partial t}\left(\alpha_q \rho_q\right) + \nabla \cdot \left(\alpha_q \rho_q \vec{v_q}\right) = 0 \tag{1}$$

where

$$\sum_{q=1}^{2} \alpha_q = 1 \tag{2}$$

The momentum equation for solid phase is:

$$\frac{\partial}{\partial t}\left(\alpha_s \rho_s \vec{v}_s\right) + \nabla \cdot \left(\alpha_s \rho_s \vec{v}_s \vec{v}_s\right) = -\alpha_s \nabla p + \nabla \cdot \overline{\overline{\tau}}_s + \alpha_s \rho_s \vec{g} + \alpha_s \rho_s \left(\vec{F}_s + \vec{F}_{\text{lift,s}} + \vec{F}_{\text{Vm,s}}\right) + \sum_{p=1}^{n} \left(K_{gs}\left(\vec{v}_g - \vec{v}_s\right) + \dot{m}_{gs} \vec{v}_{gs}\right) \tag{3}$$

where $\overline{\overline{\tau}}_s$ is the stress–strain tensor. The following equation shows that:

$$\overline{\overline{\tau}}_s = \alpha_s \mu_s \left(\nabla \cdot v_s + \nabla \cdot v_s^T\right) + \alpha_s \left(\lambda_s - \frac{2}{3}\mu_s\right) \nabla \cdot v_s \bar{\bar{I}} \tag{4}$$

$\vec{F}_s$ is an external body force. $\vec{F}_{\text{lift,s}}$ and $\vec{F}_{\text{Vm,s}}$ are lift force and virtual mass force, respectively.

$$\vec{F}_{\text{lift,s}} = -0.5 \rho_s \alpha_s \left(\vec{v}_g - \vec{v}_s\right) \times \left(\nabla \times \vec{v}_g\right) \tag{5}$$

$\vec{F}_{\text{lift,s}}$ is the lift force that affects on the secondary phase particles. These lift forces act on a particle due to velocity gradients in the primary phase flow field. The lift force would be more significant for larger particles, but the model in Fluent assumes that the particle diameter is much smaller than the interparticle spacing. In this work, the particle size is very small. Thus $\vec{F}_{\text{lift,s}}$ is set to zero, and the mass transfer is ignored.

$$\vec{F}_{\text{Vm,s}} = 0.5 \alpha_s \alpha_g \left(\frac{d_g \vec{v}_g}{dt} - \frac{d_s \vec{v}_s}{dt}\right) \tag{6}$$

The virtual mass effect is significant when the secondary phase density is much smaller than the primary phase density. Thus, it is not included in this study.

The momentum exchange between the two phases is expressed by the drag force, which is based on the gas–solid exchange coefficient K_{gs}. There are several drag models for the gas–solid interphase exchange coefficient K_{gs} in the Fluent code. The gas–solid exchange coefficient K_{gs} can be written in the following general form:

$$K_{gs} = \frac{\alpha_s \rho_s f}{\tau_s} \tag{7}$$

where f is defined differently for the different exchange-coefficient models, and τ_s, the particulate relaxation time, is defined as:

$$\tau_s = \frac{\rho_s d_s^2}{18 \mu_g} \tag{8}$$

where d_s is the diameter of particle.

f is defined generally including a drag coefficient C_D based on the relative Reynolds number (Re_s). The Syamlal and O'Brien is used:[12]

$$f = \frac{C_D Re_s \alpha_g}{24 v_{r,s}^2} \tag{9}$$

where the drag coefficient has a form derived by Dallavalle:[13]

$$C_D = \left(0.63 + \frac{4.8}{\sqrt{Re_s / v_{r,s}}}\right)^2 \tag{10}$$

This model is established based on measurements of the terminal velocities of particles in fluidized or settling beds. The correlation is a function of the gas volume fraction and relative Reynolds number.[14] The relative Reynolds number is expressed as:

$$Re_s = \frac{\rho_g d_s \left|\vec{v_s} - \vec{v_g}\right|}{\mu_g} \tag{11}$$

The interphase exchange coefficient is expressed as:

$$K_{gs} = \frac{3}{4} \frac{\alpha_s \alpha_g \rho_g}{v_{r,s}^2 d_s} C_D \left(\frac{Re_s}{v_{r,s}}\right) \left|\vec{v_s} - \vec{v_g}\right| \tag{12}$$

where $v_{r,s}$ is the terminal velocity correlation for the solid phase:[15]

$$v_{r,s} = 0.5 \left[A - 0.06 Re_s + \sqrt{(0.06 Re_s)^2 + 0.12 Re_s (2B - A) + A^2}\right] \tag{13}$$

where

$$A = \alpha_g^{4.14}$$

when

$$\alpha_g \le 0.85, \quad B = P \alpha_g^{1.28}$$

$$\alpha_g > 0.85, \quad B = \alpha_g^{Q}$$

The parameter P and Q are 0.8 and 2.65 for Fluent default, respectively. The following default equations are used to close the governing equations as seen in Table 2.

Modification of drag laws

The corresponding drag equations are empirical and would not be applicable for FCC particles investigated in this work. The Gidaspow drag law was proposed for modeling dense fluidized beds, whereas the Syamlal–O'Brien drag law had a wide range of applications.[11,16] Syamlal and O'Brien[17] introduced a method to modify their original drag law for correct simulation of the minimum fluidization conditions. Syamlal–O'Brien drag law[11] is modified using the experimental material in this study. Because P is varied with the gas superficial

Table 2. The Fluidized Bed Operating Conditions and Key Models Employed in the Simulations

Parameters	Value/Comment
Bed width (m)	0.14
Bed height (m)	1.60
Static bed height (m)	0.165
Initial void fraction solid	0.468
Time step (s)	0.0005
Coefficient of restitution	0.90
Angle of internal friction	30°
Solid pressure	Lun et al.[18]
Radial distribution	Lun et al.[18]
Shear viscosity	Syamlal[17]
Frictional viscosity	Schaeffer[19]
Granular bulk viscosity	Lun et al.

velocity, v_g is a constant (0.045 m/s) differing from the literature:

$$v_g = Re_t \frac{\alpha_g \eta_g}{d_p \rho_g} \tag{14}$$

where Re_t, Reynolds number under terminal settling conditions, is defined as:

$$Re_t = v_{r,s} Re_{ts} \tag{15}$$

$v_{r,s}$, the terminal velocity correlation, is given by:

$$v_{r,s} = \frac{A + 0.06B\,Re_{ts}}{1 + 0.06\,Re_{ts}} \tag{16}$$

Re_{ts}, the Reynolds number under terminal settling conditions for a single particle, is given by:

$$Re_{ts} = \left(\frac{\sqrt{4.8^2 + 2.52\sqrt{4Ar/3}} - 4.8}{1.26} \right)^2 \tag{17}$$

Ar, the Archimedes number, is given by:

$$Ar = \frac{(\rho_s - \rho_g) d_s^3 \rho_g g}{\eta_g^2} \tag{18}$$

The parameter Q is modified according to equation:

$$Q = 1.28 + \log(P)/\log(0.85) \tag{19}$$

Acoustic models

Herrera and Levy[20] found that sound wave transmission had a standing wave through a column. In acoustic fluidized bed, the sound energy exerts a force on the particles through sound wave transmission. Considering the effect of sound field on particles, it is assumed that the vibration velocity produced by sound wave acting on the particles is expressed as $U \sin \omega t$. The total gas velocity V acting on the particles equals to the superficial gas velocity U_G adding to the vibration velocity $U \sin \omega t$ in acoustic fluidized bed.[21]

$$V = U_G + U \sin \omega t \tag{20}$$

where the velocity peak value U produced by sound wave is calculated by:[22]

$$\mathrm{SPL} = 20 \log \frac{U}{\sqrt{2} U_{ref}} \tag{21}$$

where U_{ref} is the reference velocity and $U_{ref} = 4.83 \times 10^{-8}$ m/s in this study. SPL is the sound pressure level, which is the amplitude of acoustic pressure compressed to a logarithmic scale and referred to the threshold of human hearing, is expressed by:[23]

$$\mathrm{SPL} = 20 \log \left[\frac{P_{rms}}{P_{ref}} \right] \tag{22}$$

where the root mean square of sound P_{rms} refers to the overall measurement of the amplitude of the sound pressure defined by:[20]

$$P_{rms} = \frac{|P(x,t)|}{\sqrt{2}} = \frac{P}{\sqrt{2}} \tag{23}$$

where P is the absolute magnitude of the sound pressure, $P = |P(x,t)|$.

P_{ref} is the reference pressure, which is chosen to be the value at the threshold of human hearing and $P_{ref} = 2 \times 10^{-5}$ Pa.

In Eq. 3, $\vec{F}_s$ is an external body force. It will be added to the right-hand side of the momentum equation for solid phase if the solid is affected by other external forces. The particles in the acoustic fluidized bed are influenced by sound field. The momentum equation of particles in the sound field based on the Stokes formula[21] is expressed by:

$$\frac{du_s}{dt} = \frac{u_g - u_s}{\tau_s} \tag{24}$$

τ_s is particle relaxation time, which is related to the particles size and fluid viscosity as seen in Eq. 8.

Where u_g and u_s are gas and particle velocities, respectively. When the oscillation velocity of gas medium is much smaller than sound velocity ($U/c \ll 1$), the particle semidiameter is much smaller than sound wavelength ($d_s/2\lambda \ll 1$), and the shape of incidence sound wave is simple harmonic oscillation, u_g and u_s can be presented as following:[21]

$$u_g = U \sin(\omega t) \tag{25}$$

$$u_s = \eta_s U \sin(\omega t - \phi) \tag{26}$$

where η_s is acoustic entrainment coefficient of particle, ϕ is phase difference between gas and particle movement, which can be presented as:

$$\eta_s = \frac{1}{\sqrt{1 + \omega^2 \tau_s^2}} \tag{27}$$

$$\phi = \tan^{-1}(\omega\tau_s) \tag{28}$$

The velocity difference between gas and particles is presented as:

$$u_{gs} = u_g - u_s = \eta_{gs} U \cos(\omega t - \phi) \tag{29}$$

where η_{gs} is the relative slip coefficient between gas and particles, it is calculated by:

$$\eta_{gs} = \frac{\omega\tau_s}{\sqrt{1+\omega^2\tau_s^2}} \tag{30}$$

The particle momentum in sound field can be added to the original momentum equation based on the aforementioned analysis. However, the analysis is based on the single particle from Stokes formula, and it is used for dilute fluidized bed. It should be corrected in dense fluidized bed. Comparing with solid phase, the effect of sound field on the gas phase is insignificant in the dense phase region of gas–solid fluidized bed, the gas velocity (u_g) can be ignored. The momentum equation of fine particles in sound field fluidized bed can be modified as:

$$\frac{du_s}{dt} = \frac{-u_s}{\tau_s} \tag{31}$$

The analysis process is the same as mentioned earlier, and Eq. 31 can be presented as:

$$\frac{d(\alpha_s u_s \rho_s)}{dt} = \rho_s \alpha_s \left(\frac{-u_s}{\tau_s}\right) = -\frac{\rho_s \alpha_s}{\tau_s} \eta_s U \sin(\omega t - \phi) \tag{32}$$

where α_s, solid volume fraction, changes with time. The momentum equation in the acoustic fluidized bed is given as follows:

$$\frac{\partial}{\partial t}\left(\alpha_s \rho_s \vec{v}_s\right) + \nabla \cdot \left(\alpha_s \rho_s \vec{v}_s \vec{v}_s\right) = -\alpha_s \nabla p + \nabla \cdot \overline{\overline{\tau_s}} + \alpha_s \rho_s \vec{g} - \frac{\rho_s \alpha_s}{\tau_s} \eta_s U \sin(\omega t - \phi) + K_{gs}\left(\vec{v}_g - \vec{v}_s\right) \tag{33}$$

As the complexity of the gas–solid system, the user-defined source terms, $\vec{F}_s$, is added to the original solid momentum equation which is even more complex. The calculation time for acoustic fluidized bed is much longer than that for conventional one. Thus, the added equation should be as linear as possible to get the stability results. α_s is chosen as 0.45 based on experimental conditions in this study.

Numerical method

A commercial CFD code, Fluent 6.2, was used to simulate the flow property of acoustic fluidized bed. To solve the differential governing equations presented earlier numerically, discretion of equations was made by a finite volume scheme. The coupling between pressure and velocity used the SIMPLEC method proposed by Patanker and Spalding.[24] The second-order upwind and QUICK discretization schemes were used for momentum and volume fraction equations, respectively. A no-slip condition is accepted at the wall region.

Boundary conditions

The operation conditions and model parameters were summarized in Table 2. The time taken was controlled by the geometry model and numbers of the grid in the calculation. The size of the cells should have been fine sufficiently so that the change of flow properties across the cell was small. The main object was to investigate the effect of sound assistance on the particles fluidization characteristics and validate the acoustic model. The simulations for gas–solid flow systems were carried out in a two-dimensional rectangular space to reduce computational time.[25] The divided network cells were achieved using quadrilateral body structure, but the distributor region was drawn specific grid to reduce the error produced by grid. The distributor grid size was 0.001×0.001 m^2, and the other region was 0.003×0.003 m^2. This simplification reduced the computational costs drastically while the influence of the simulation results was negligible.

The superficial gas velocity was specified as uniform across the inlet along the axial direction, whereas the particle volume fraction at the inlet was specified as zero. The vibration velocity produced by sound wave was specified after programmed. The upper part of the reactor was freeboard, which was high enough at the top to make sure that the particle concentration was negligible. The FCC particles, which were assumed to be a group of sphere particles with the same density and size, were packed above the distributor previously with the void of 0.532. The restitution coefficient used in the simulations was 0.9. It was indicated that the particles were assumed nearly elastic.[26]

We found that it will take up to 5 s of simulating time to gain the time-independent average profiles in two-dimensional simulations. Then the reactor behavior reached the steady state. This can ensure that the behavior of a bubbling bed was not that of startup. Considering the number of grid cells used in this study, however, the simulations were run for 10 s of real time. The average results were obtained from the last 5 s.

Results and Discussion

Effect of drag models on radial particle volume fraction

It is shown in Figure 2 that the simulation results of radial particle volume fraction using the original Syamlal–O'Brien drag model and the modified one under the same operating conditions. It can be found that the radial particle volume fraction using modified drag model was larger than that for the original one, but the change trends were the same. The particle volume fraction decreased from the wall region to the center, and they presented parabolic concentration profile along radial direction.

It was indicated that the initial Syamlal–O'Brien drag model had an overestimation of the drag force. The discrepancy between the simulation and experimental results was due to the cohesive interparticle forces, which was responsible for agglomeration of particles resulting in a decrease of drag force for FCC particles. It can lead to a higher drag force, larger size bubbles, and higher bed expansion without considering the effects of cohesive forces and agglomeration.

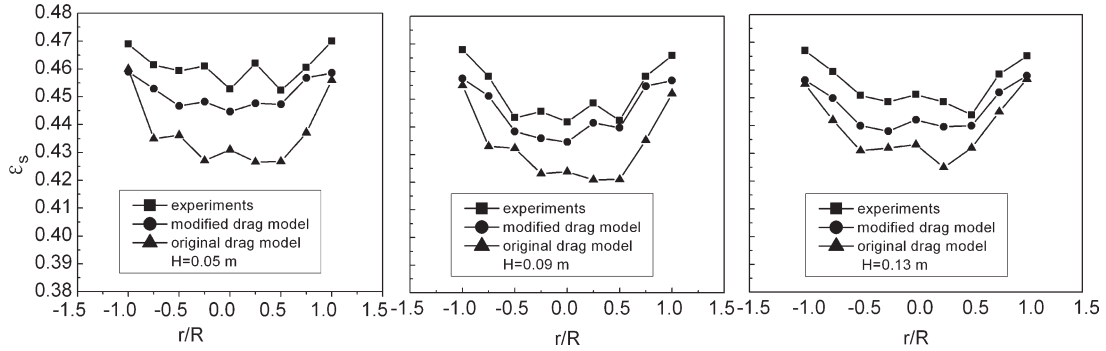

Figure 2. Radial direction time-averaged particle volume fraction distribution without sound assistant (U_G = 0.045 m/s, H_0 = 0.165 m).

Similar overestimations were observed by other researchers.[11,27,28] Because the drag model coefficients were varied with the fluidized velocity, the method employed to modify the Syamlal–O'Brien drag model was based on the operation velocity, $U_G = 0.045$ m/s, which was different from it in the literature.[11] From Eq. 12, K_{gs} decreased with increasing $v_{r,s}$. A and B decreased with increasing P and Q because gas void α_g was smaller than 1.0 at all time. In this study, $P = 1.364$, $Q = -0.63$, which were different from the default values ($P = 0.8$, $Q = 2.65$).

It can also be observed from Figure 2 that the results obtained from Syamlal–O'Brien drag model and the modified one had the same profile of particle volume fraction. It was consistent with the particle distribution trend in conventional fluidized bed. Because the investigation of acoustic fluidized bed was based on the conventional fluidized bed, it was advantageous to decrease calculated error in acoustic fluidized bed as calculated error in conventional fluidized bed was decrease. So, the following investigation into the effect of sound field on fluidization behaviors was based on the modified Syamlal–O'Brien drag model.

Effect of sound pressure level on particle volume fraction

Figure 3 showed the time-averaged particle volume fraction distribution using simulation and experiment with sound assistance (SPL = 90, 100, 110, 120, 130 dB, $f = 100$ Hz). It can be found from Figure 3 that the experimental and simulated values of particle volume fraction were different. However, they had the same change trend. The local particle volume fraction increased with increasing sound pressure level, but it was little influenced by sound field at the wall region. The particle volume fraction decreased from the wall region to the center, and they revealed parabolic profile along radial direction.

Figures 2 and 3 showed that particle volume fraction had obvious variation along radial direction. A minimum value of particle volume fraction displayed in the center region of the reactor, which indicated that large bubbles appeared or the particles were compacted in the center region. It should be pointed out that the phenomena mentioned earlier were not taken into account sound assistance. It can also be found from Figure 3 that the particle volume fraction increased with increasing sound pressure level far away from the wall and the change curve was gradually smooth (r/R = 0–1.0). The reason was that sound energy was absorbed by particles in fluidized bed and part of cohesive force was resisted. Thus, fluidization quality was improved. The definition of sound energy was given by:[23]

$$E_{sou} = \frac{1}{4}\pi d_a^2 I = \frac{1}{4}\pi d_a^2 k_a 10^{-12+\mathrm{SPL}} \left(\frac{f}{f_c}\right)^n e^{(\mathrm{SPL}-\mathrm{SPL}_c)/\mathrm{SPL}_c} \quad (34)$$

It can be found from Eq. 34 that sound energy increased with increasing sound pressure level as sound frequency was a constant, which agreed with Figure 3. However, from comparison of the particle volume fraction under different sound pressure levels shown in Figures 3a, d, it was clearly found that the sound wave had a less effect on the particle volume fraction near wall region and bed bottom region. At the wall region, the particle movement was affected by the wall effect and the external sound energy had little effect on the particle volume fraction. The particle volume fraction near bed bottom region ($H = 0.05$ m) increased with increasing sound pressure level, but the trend was not obvious. The reason was that when an acoustic wave propagated through a medium, acoustic wave intensity reduced owing to the attenuation effect of the medium. The attenuation variation can be described by the following relationship:[29]

$$\mathrm{SPL} \propto \mathrm{SPL}_0 l^{-2} e^{-2\alpha l} \quad (35)$$

where SPL_0 was the initial sound pressure level, SPL was the local sound pressure level when acoustic wave propagated in the medium for propagating distance of acoustic wave (l), and α was the attenuation coefficient. Equation 35 demonstrated the exponential decrease of the sound pressure level with increasing propagating distance of acoustic wave. The sound energy attenuated gradually as the sound wave propagated from the upper region to bottom region. Then the insufficient sound energy cannot break up the bubbles.

Figure 4 was the contours of particle instantaneous volume fraction under different sound pressure levels. It can be observed from Figure 4 that the bubble size decreased and the number of the bubbles increased with increasing sound pressure level.

Guo et al.[23] found that the external energy input by sound wave was propitious to break up the ultrafine particle

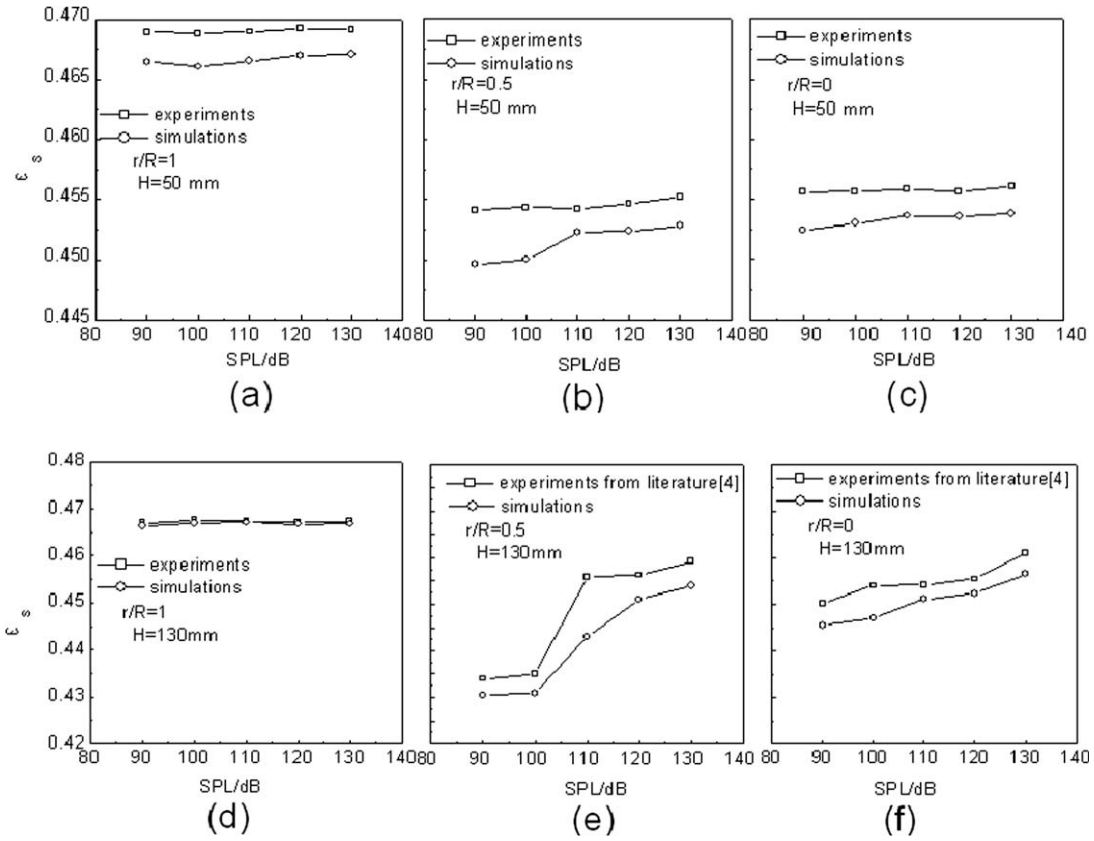

Figure 3. Radial direction time-averaged solid concentration distribution against sound pressure levels (U_G = 0.045 m/s, H_0 = 0.165 m, f = 100 Hz).

agglomerates at a low sound pressure level. At the same time, the sound wave increased the contact possibility between particles and agglomerates, which caused large size agglomerate at high sound pressure level. However, the result of sound excitation on Geldart type A particles was different from Geldart type C, because the interparticle cohesive force for Geldart type A particles was much smaller than that for Geldart type C particles. The present investigation showed that the sound energy can break up larger bubbles into smaller ones for the FCC particles in an acoustic fluidized bed. The results in Figure 4 agreed with the results discussed earlier in Figure 3.

Equation 12 demonstrated that K_{gs} was influenced by gas and solid velocities. Gas velocity, induced by sound assistance, could change as the form of sine wave.[30] The variation of particle velocity in the sound field was discussed in the following section. As discussed earlier, the gas and solid volume fractions were all influenced by sound assistance. Syamlal–O'Brien drag model used in the conventional fluidized bed would be changed in the acoustic fluidized bed.

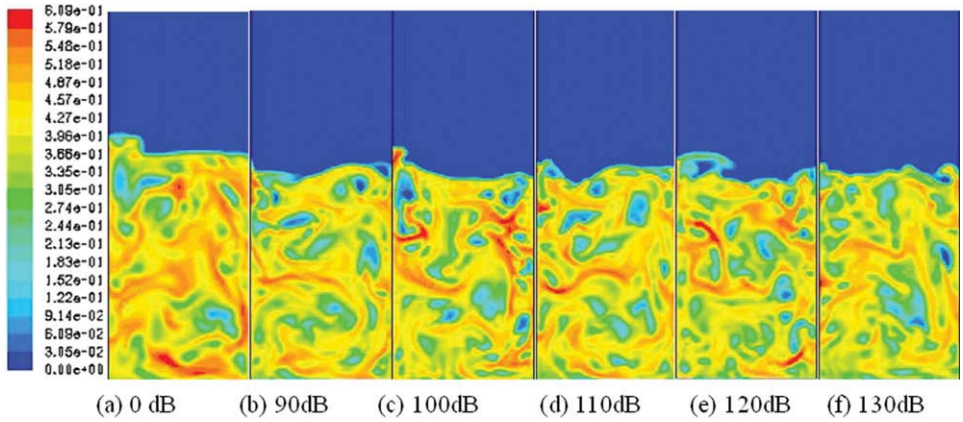

Figure 4. Contours of solid instantaneous volume fraction against sound pressure levels (U_G = 0.045 m/s, H_0 = 0.165 m, f = 100 Hz, t = 8 s).

[Color figure can be viewed in the online issue, which is available at www.interscience.wiley.com.]

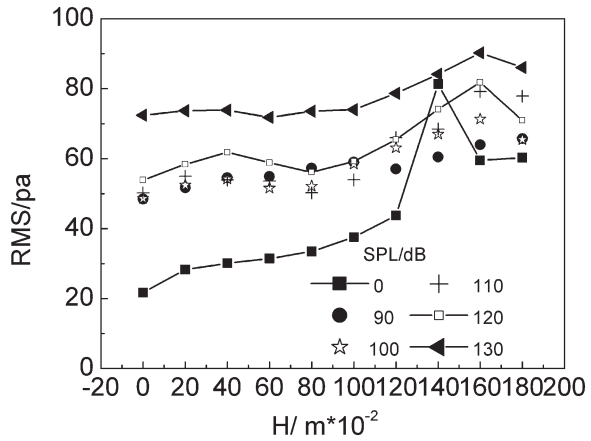

Figure 5. Axial RMS of bed pressure drop against different sound pressure levels (U_G = 0.045 m/s, H_0 = 0.165 m, f = 100 Hz, t = 8 s).

The affection factor in drag model was complex, such as gas and particle volume fractions, gas and particle velocities. The drag force decreased with increasing sound pressure level, which caused the bubble size decrease and particle volume fraction increase. Because Eq. 12 was nonlinear, and the momentum equation in the acoustic fluidized bed was complex, it was significant to investigate the behavior of the acoustic fluidized bed further.

Effect of sound pressure level on RMS of bed pressure drop

Root-mean-square (RMS) of bed pressure drop is proportion to pressure fluctuation. The increase of RMS indicates an increase of the frequency of bubble coalescence or breakup and the drag force acting on the particles. Thus, the heterogeneous characteristic of flow structure is enhanced. Pressure fluctuation is an important parameter in the design and operation of fluidized bed reactor, which contains a lot of characteristics inside the fluidized bed reactor. From earlier discussion, the present numerical model can predict the bed pressure drop characteristics. Thus, the RMS of bed pressure drop at different bed heights can be calculated using CFD approach. The instantaneous bed pressure drop can be analyzed as:

$$\Delta p = \Delta\overline{p} + \Delta p' \tag{36}$$

where $\Delta\overline{p}$ is the average pressure drop, which is constant under the present operation condition, and $\Delta p'$ is the fluctuating value which is a stochastic variable and equals zero under the present condition. The RMS value is equal to the standard deviation value when the average value of stochastic variable is zero based on the statistical theory.[31] The RMS of $\Delta p'$ is calculated as follows:

$$\sigma_p = \sqrt{\frac{1}{N}\sum_{i=1}^{N}(\Delta p_i - \Delta\overline{p})^2} \tag{37}$$

Figure 5 exhibited the comparison of RMS of bed pressure drop along the bed height under different sound pressure levels (SPL = 0, 90, 100, 110, 120, 130 dB). It showed that the RMS of bed pressure drop increased with increasing bed height initially and then decreased at the location of exceeding the static bed height. The global RMS of bed pressure drop increased with increasing sound pressure level. It had an obvious maximum value at the top of fluidized bed without sound assistance. The reason was that larger bubbles were formed due to bubble coalescence with bubble rising, which caused the RMS of bed pressure drop increased along bed height without external disturbing action. The RMS of bed pressure drop decreased near bed top of exceeding the static bed height because of bubble breakup. Under external sound energy, the larger bubbles near the top of the bed can be broken into small ones, the variation of RMS was not abrupt. The phenomenon, RMS increased with increasing sound pressure level, showed that the sound energy and the particle fluctuation energy all increased with increasing sound pressure level. Then, the frequency of bubble breakup increased, and the RMS caused by bubble behaviors is enlarged. Figure 5 indicated that the RMS of bed pressure drop in acoustic fluidized bed had drop points before arriving bed top, but kept on increasing after that point. The reason was unclear. It was probably caused mainly by the bubble breakup earlier with external sound energy. Abed[32] found the similar phenomenon in gas–solid fluidized bed without external energy.

Effect of sound pressure levels on granular temperature

Equivalent to the thermodynamic temperature for gases, the granular temperature can be introduced as a measurement for the energy of the particles' fluctuating velocity. The granular temperature is defined as:[26]

$$\Theta_s = \frac{1}{3}v_s'^2 \tag{38}$$

where Θ_s is the granular temperature, and v_s' is the particle fluctuating velocity. The equation of conservation of the particle fluctuating energy can be described in Ding and Gidaspow:[33]

$$\frac{3}{2}\left[\frac{\partial}{\partial t}(\rho_s\alpha_s\Theta_s) + \nabla\cdot\left(\rho_s\alpha_s\vec{v}_s\Theta_s\right)\right] = \left(-p_s\bar{\bar{I}} + \overline{\overline{\tau_s}}\right):\nabla\vec{v}_s + \nabla\cdot(k_{\Theta_s}\nabla\Theta_s) - \gamma\Theta_s + \phi_{gs} \tag{39}$$

where $\left(-p_s\bar{\bar{I}} + \overline{\overline{\tau_s}}\right):\nabla\vec{v}$ is the generation of energy by the particle stress tensor, $k_{\Theta_s}\nabla\Theta_s$ is the diffusion of energy, $\gamma\Theta_s$ is the collisional dissipation of energy, ϕ_{gs} is the energy exchange between the fluid or solid phase and the solid phase. In this work, the algebraic model was used to calculate the granular temperature. The model assumed that the granular energy was dissipated locally and only generation and dissipation terms were retained. The procedure had been proven by simulations of noncirculating beds.[34]

Figure 6 showed the comparison of the average granular temperature (Θ_s) in an acoustic fluidized bed under different sound pressure levels (SPL = 0, 90, 100, 110, 120, 130, f = 100 Hz). It can be found from Figure 6 that Θ_s increased with increasing sound pressure levels. In Eq. 39, ϕ_{gs}, the transfer of the kinetic energy of random fluctuation in

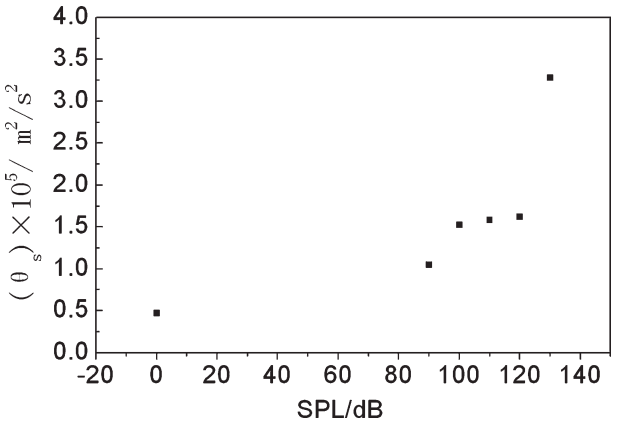

Figure 6. Granular temperature against sound pressure levels (U_G = 0.045 m/s, f = 100 Hz, H_0 = 0.165 m).

particle velocity from the solid phase to gas phase or solid phase, was represented:[16]

$$\phi_{gs} = -3K_{gs}\Theta_s \tag{40}$$

When the external sound energy is introduced as vibration velocity to solid particles, the kinetic energy of random fluctuation between gas and particles enhanced. The sound energy increased with increasing sound pressure level, and the particle vibration velocity increased. Thus, it can be deduced from Eq. 40 that Θ_s increased, which coincided with the simulation results in Figure 6.

It can be seen from solid momentum Eq. 33 that the solid momentum caused by sound field was added in the original momentum equation. The added term was the form of sine wave, and the solid fluctuation velocity increased the effect of sound filed. It was known from earlier discussion that the efficiency of sound filed on particles increased with increasing sound pressure level. Thus, the particle fluctuation velocity caused by sound field increased, and further the granular temperature increased with increasing sound pressure level. However, the results in this work were different from the investigation of Jung et al.,[35] and granular temperature decreased with an increase of the particle volume fraction. In the present work as displayed earlier, the local particle volume fraction increased with increasing sound pressure level. Because the granular temperature depended on the particle size, flow patterns, gas velocity and other parameters, the acoustic models established in this work need to be modified further.

Effects of sound pressure levels on particle velocity

Figure 7 showed typical vertical and lateral instantaneous particle velocity profiles in the center region (r = 0.07 m)

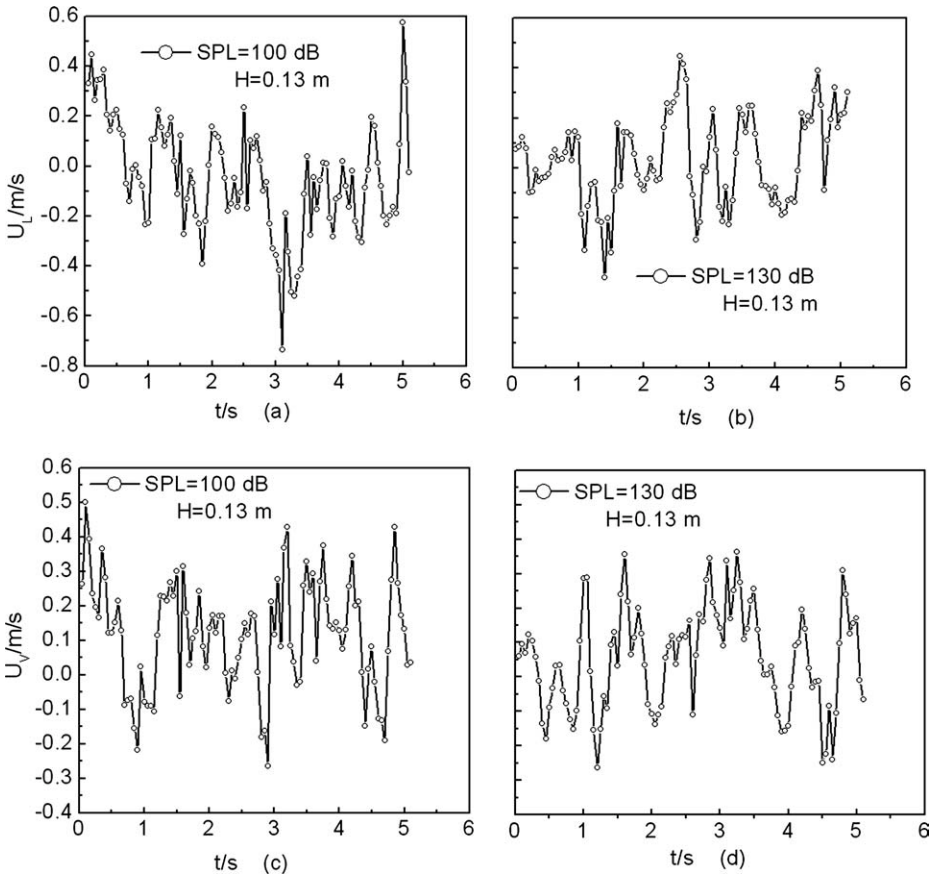

Figure 7. Typical time series of vertical (a, b) and lateral (c, d) velocities for particles in the center region. (U_G = 0.045 m/s, H_0 = 0.165 m, H = 0.13 m, r = 0.07 m, f = 100 Hz).

with a bed height of 0.13 m under different sound pressure levels. The effectiveness of sound pressure level was clearly demonstrated in Figure 7. The particle velocity magnitudes increased with decreasing sound pressure level. The reason was that the bubble size decreased with increasing sound pressure level. It was known that bubbles were the main driving force for particle movement in bubbling beds. When large bubbles appeared in the acoustic fluidized bed, the local velocity of particles increased as shown in Figures 7a,c. The change trend of particle velocity was smoother with increasing SPL, as seen in Figures 7b,d. A relationship between bubble size and bubble rise velocity was obtained from bubble theory. Davidson and Harrison[36] proposed the semiexperience correlation to calculate single bubble rise velocity in bubbling beds, which was given as:

$$\overline{u}_{\mathrm{b}} = u - u_{mf} + 0.71\sqrt{g\overline{D}_{\mathrm{b}}} \tag{41}$$

It was found from Eq. 41 that the bubble rise velocity increased with increasing average bubble size. Furthermore, the force of driving particle motion increased. The velocity magnitude of neighborhood particles to large bubbles was larger the effect of larger bubbles. This was consistent with the conclusion obtained earlier.

Thus, the discussion in this section was reliable, and the sound pressure level had an important effect on particle movement. With an increase of sound pressure level, the change trend of global particle velocity was smooth. The reason was that the sound energy broke up large size bubbles into small ones in the acoustic fluidized bed, and reduced the local particle velocity. The movement frequency of particles increased in the sound filed. Thus, the solid fluctuation energy increased. Anyway, the acoustic model established in this work can describe adequately the effect of sound assistance on the fluidization characteristics.

Conclusion

In our work, Syamlal–O'Brien drag model was modified and an acoustic model was established for gas–solid fluidized bed in CFD code Fluent 6.2.

(1) The radial particle volume fraction in conventional fluidized bed, which was calculated by modification drag model of Syamlal–O'Brien, increased comparing with that by the original one. The distribution of radial and axial particle volume fraction was consistent with that using the original drag model, and the discrepancy between simulated data and experimental values decreased. The modified drag model was reliable.

(2) The established acoustic model was investigated using CFD code Fluent 6.2. The radial particle volume fraction increased with increasing sound pressure level, and the wall region had little effect of sound pressure level. The bubble size decreased and the number of bubbles increased with increasing sound pressure levels.

(3) The RMS of bed pressure drop increased with increasing sound pressure levels, and the frequency of bubble coalescence and breakup also increased.

(4) The extension of particle velocity in vertical and lateral direction decreased with increasing sound pressure level. However, the granular temperature, which was used to describe the energy of the fluctuating velocity of the particles, increased with increasing sound pressure levels.

(5) The simulation results were compared with experimental data or the literature investigation. The established acoustic model can describe the effect of sound assistant on fluidization characteristics of gas–solid fluidized bed.

Acknowledgments

This work was supported by Taishan Mountain Scholar Constructive Engineering Foundation of China (Js200510036), National Natural Science Foundation of China (20676064), and Young Scientist Awarding Foundation of Shandong Province (2006BS08002).

Notation

Ar = Archimedes number (dimensionless)
C_{D} = drag coefficient (dimensionless)
D = column diameter (m)
D_{b} = average bubble size at the bed height H (m)
d_{s} = the diameter of particles (m)
E_{sou} = the energy generated by sound assistance (w/m^3)
e_{ss} = coefficient of restitution for particle collisions (dimensionless)
$\vec{F}_{\mathrm{lift}}$ = lift force (N)
$\vec{F}_{\mathrm{Vm,s}}$ = virtual mass force (N)
f = sound frequency (Hz)
H = column height (m)
H_0 = static bed height (m)
$I_{2\mathrm{D}}$ = the second invariant of the deviatoric stress tensor (dimensionless)
K_{gs} = gas–solid exchange coefficients (dimensionless)
p_{s} = solid phase pressure (Pa)
$\Delta p'$ = fluctuating pressure drop (Pa)
$\Delta\overline{p}$ = average pressure drop (Pa)
Δp = the instantaneous bed pressure drop (Pa)
Re_{s} = solid-phase Reynolds number (dimensionless)
Re_{t} = the Reynolds number under terminal settling conditions (dimensionless)
Re_{ts} = Reynolds number under terminal settling conditions for a single particle (dimensionless)
SPL = sound pressure level (dB)
t = time (s)
U = velocity peak value produced by sound wave (m/s)
U_{G} = superficial velocity (m/s)
U_{L} = lateral velocity (m/s)
u_{mf} = minimum fluidized velocity (m/s)
U_{V} = vertical velocity (m/s)
$\overline{u}_{\mathrm{b}}$ = bubble rise velocity (m/s)
$v_{\mathrm{r,s}}$ = the terminal velocity (m/s)
α = sound energy attenuation coefficient in Eq. 35 (dimensionless)
α_{s} = solid volume fraction (dimensionless)
α_{g} = gas volume fraction (dimensionless)
Θ_{s} = solid granular temperature (m^2/s^2)
$\overline{\overline{\tau_{\mathrm{s}}}}$ = the solid stress–strain tensor (Pa)
τ_{s} = particulate relaxation time (s)
μ_{s} = solid stress viscosity (Pa s)
λ_{s} = solid bulk viscosity (Pa s)
λ = sound wavelength (m)
η_{s} = acoustic entrainment coefficient of particle (dimensionless)
ϕ = phase difference between gas and solid particle movement (dimensionless)

Literature Cited

1. Herrera CA, Levy EK. Bubbling characteristics of sound-assisted fluidized bed. *Powder Technol*. 2001;119:229–240.
2. Morse RD. Sonic energy in granular solid fluidization. *Ind Eng Chem Res*. 1955;47:1170–1175.
3. Levy EK, Shnitzer I, Masaki T, Salmento J. Effect of an acoustic field on bubbling in a gas fluidized bed. *Powder Technol*. 1997;90: 53–57.

4. Guo QJ, Liu HE, Shen WZ, Yan XH, Jia RG. Influence of sound wave characteristics on fluidization behaviors of ultrafine particles. *Chem Eng J*. 2006;119:1–9.
5. Xu ZF, Khoo BC, Carpenter K. Mass transfer across the turbulent gas-water interface. *AIChE J*. 2006;52:3363–3374.
6. Xu ZF, Khoo BC, Wijeysundera NE. Mass transfer across the falling film: simulations and experiments. *Chem Eng Sci*. 2008;63:2559–2575.
7. Sharma SD, Pugsley T. Three-dimensional CFD model of the deaeration rate of FCC particles. *AIChE J*. 2006;52:2391–2400.
8. Syamlal M, O'Brien TJ. Fluid dynamic simulation of O_3 decomposition in a bubbling fluidized bed. *AIChE J*. 2003;49:2793–2801.
9. Wang HG, Yang WQ. Study of bubbling and slugging fluidized beds by simulation and ECT. *AIChE J*. 2006;52:3078–3087.
10. Si CD, Guo QJ, Cui CX. Investigation into particle concentration of Geldart group A in an acoustic fluidized bed. *Chem React Eng Technol*. 2008;24:12–17.
11. Zimmermann S, Taghipour F. CFD modeling of the hydrodynamics and reaction kinetics of FCC fluidized-bed reactors. *Ind Eng Chem Res*. 2005;44:9818–9827.
12. Syamlal M, O'Brien TJ. Computer simulation of bubbles in a fluidized bed. *AIChE Symp Ser*. 1989;85:22–31.
13. Dallavalle JM. *Micromeritics*. London: Pitman, 1948.
14. Richardson JR, Zaki WN. Sedimentation and fluidization: Part I. *Trans Inst Chem Eng*. 1954;32:35–53.
15. Garside J, Al-Dibouni MR. Velocity-voidage relationships for fluidization and sedimentation. *Ind Eng Chem Proc Des Dev*. 1977; 16:206–214.
16. Lee SY, Richard AD. *FLUENT 6.2 Documentation*. Lebanon, NH: Fluent Inc., 2005; Section 24.4, Eulerian Model.
17. Syamlal M, O'Brien TJ. *Derivation of a Drag Coefficient from Velocity-Voidage Correlation*. U.S. Department of Energy, Office of Fossil Energy, National Energy Technology Laboratory,Morgantown, WV, 1987.
18. Lun CKK, Savage SB, Jeffrey DJ, Chepurniy N. Kinetic theories for granular flow: Inelastic particles incouette flow and slightly inelastic particles in a general flow field. *J Fluid Mech*. 1984;140:223–256.
19. Schaeffer DG. Instability in the evolution equations describing incompressible granular flow. *J Diff Eq*. 1987;66:19–50.
20. Herrera CA, Levy EK. Characteristics of acoustic standing waves in fluidized beds. *AIChE J*. 2000;48:503–513.
21. Fuchs NA. *Aerosols Dynamics*. Beijing: Science Press, 1960.
22. Chirone R, Massinina L, Russo S. Bubble-free fluidization of a cohesive powder in an acoustic field. *Chem Eng Sci*. 1993;48:41–52.
23. Guo QJ, Yang XP, Shen WZ, Liu HE. Agglomerate size in an acoustic fluidized bed with sound assistance. *Chem Eng Process*. 2007;46:307–313.
24. Patanker SV, Spalding DB. A calculation procedure for heat, mass and momentum transfer in three-dimensional parabolic flows. *Int J Heat Mass Transfer*. 1972;15:1787–1806.
25. Hulme I, Clavelle E, van der Lee L, Kantzas A. CFD modeling and validation of bubble properties for a bubbling fluidized bed. *Ind Eng Chem Res*. 2005;44:4254–4266.
26. van Wachem B, Sasic S. Derivation, simulation, and validation of a cohesive particle flow CFD model. *AIChE J*. 2008;54:9–19.
27. McKeen T, Pugsley T. Simulation and experimental validation of a freely bubbling bed of FCC catalyst. *Powder Technol*. 2003;129: 139–152.
28. Ferschneider G, Mege P. Eulerian simulation of dense phase fluidized beds. *Rev Inst Fr Pet*. 1996;51:301–307.
29. Wu D, Qian Z, Shao D. Sound attenuation in a coarse granular medium. *J Sound Vib*. 1993;162:529–535.
30. Liang HQ. Study on Fluidization Characteristics of Fine Particles in a Sound-Assisted Fluidized Bed, M.Sc Thesis. China: Sichuan University, 2003.
31. Zhou ZY, Shi YF, Yu HR. Discrimination between particulate and aggregative fluidization by pressure fluctuation. *Chem React Eng Technol*. 1999;15:262–267.
32. Abed R. Characterization of hydrodynamic nonuniformity in large fluidized beds. *Ind Eng Chem Fundam*. 1985;24:78–82.
33. Ding J, Gidaspow D. A bubbling fluidization model using kinetic theory of granular flow. *AIChE J*. 1990;36:523–538.
34. Wachem BGM, Schouten JC, van den Bleek CM, Krishna R, Sinclair JL. Comparative analysis of CFD models of dense gas-solid systems. *AIChE J*. 2001;46:1035–1051.
35. Jung J, Gidaspow D, Gamwo IK. Measurement of two kinds of granular temperatures, stresses, and dispersion in bubbling beds. *Ind Eng Chem Res*. 2005;44:1329–1341.
36. Davidson JF, Harrison D. *Fluidized Particles*. Cambridge: Cambridge University Press, 1963.

Manuscript received Dec. 18, 2008, and revision received Sept. 16, 2009.